JOURNAL OF CHEMICAL INFORMATION AND MODELING

Article

pubs.acs.org/jcim

Switchable Nonlinear Optical Properties of η^5-Monocyclopentadienylmetal Complexes: A DFT Approach

Paulo J. Mendes,*[,‡] Tiago J. L. Silva,[†,‡] M. Helena Garcia,[†] J. P. Prates Ramalho,[‡] and A. J. Palace Carvalho[‡]

[†]Centro de Ciências Moleculares e Materiais, Faculdade de Ciências da Universidade de Lisboa, Campo Grande, 1749-016 Lisboa, Portugal

[‡]Centro de Química de Évora, Universidade de Évora, Rua Romão Ramalho 59, 7002-554 Évora, Portugal

Supporting Information

ABSTRACT: Density functional theory (DFT) calculations have been carried out to investigate the switching of the second-order nonlinear optical (NLO) properties of η^5-monocyclopentadienyliron(II) and ruthenium(II) model complexes presenting 5-(3-(thiophen-2-yl)benzo[*c*]thiophen-1-yl)-thiophene-2-carbonitrile as a ligand. The switching properties were induced by redox means. Both oxidation and reduction stimulus have been considered, and calculations have been performed both for the complexes and for the free benzo[*c*]-thiophene derivative ligand in order to elucidate the role played by the organometallic fragment on the second-order NLO properties of these complexes. B3LYP, CAM-B3LYP, and M06 functionals were used for our calculations. The results show some important structural changes upon oxidation/reduction that are accompanied by significant differences on the corresponding second-order NLO properties. TD-DFT calculations show that these differences on the second-order NLO response upon oxidation/reduction are due to a change in the charge transfer pattern, in which the organometallic iron and ruthenium moieties play an important role. The calculated static hyperpolarizabilities were found to be strongly functional dependent. CAM-B3LYP, however, seems to predict more reliable structural and optical data as well as hyperpolarizabilities when compared to experimental data. The use of this functional predicts that the studied complexes can be viewed as acting as redox second-order NLO switches, in particular using oxidation stimulus. The β_{tot} value of one-electron oxidized species is at least ~8.3 times (for Ru complex) and ~5.5 times (for Fe complex) as large as that of its nonoxidized counterparts.

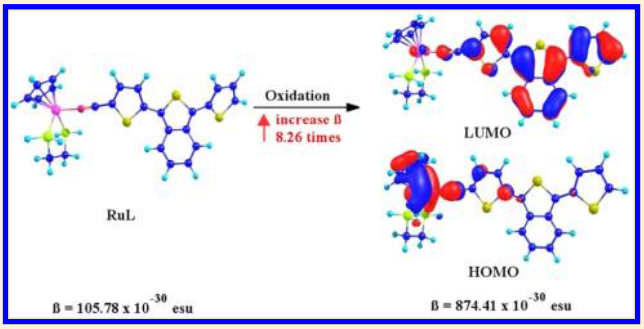

1. INTRODUCTION

Molecular switches have attracted a great attention in the last years owing to their potential use as key nanoscale components for digital processing and communication.[1] To date, molecular switches have been reported exhibiting changes in properties such as color,[2] luminescence,[3] magnetic properties,[4] and optical nonlinearity (NLO).[5,6]

Although fundamental research for NLO properties have been mostly devoted to the preparation of compounds with large optical nonlinearities, the use of these properties in view of the molecular switching has attracted considerable interest, and some reviews have been published.[5−8] In the context of NLO properties, transition organometallic/coordination compounds revealed encouraging results because they possess large optical nonlinearities and fast response times. In addition, the diversity of metal centers, oxidation states, ligand environments, and coordination geometries allow to fine-tune the second-order NLO (SONLO) response. Indeed, the presence of a redox-active metal center within a conjugated system provides excellent opportunities for a reversible modulation of the SONLO properties. This makes it possible to achieve a redox switch in the SONLO response between two forms ("on" and "off") because they often have a great difference in the magnitude of the corresponding first hyperpolarizabilities (β). Most of the studies concerning the redox-switchable molecules have been made on iron/ruthenium pyridine coordination compounds, electron-rich ferrocenyl derivatives, and piano stool complexes presenting benzene-based spacers.[5−8] These examples mostly exploit the redox behavior of the donor fragment and are based on a type I switching mechanism (lowering of the donor capacity of the "on" form by oxidation).[5] In this mechanism, the donor becomes a competing acceptor moiety (A′) thus leading to lower hyperpolarizability ("off" form). Typically, these complexes are push−pull systems in which the metal center, bonded to a hyperpolarizable organic conjugated backbone, acts as an electron-donor group in a dipolar donor/conjugated bridge/acceptor (D-π-A) structure. However, Weyland et al.[9] have investigated the effect of oxidation state on the second-order

Received: May 10, 2012
Published: July 26, 2012

dx.doi.org/10.1021/ci300226t | *J. Chem. Inf. Model.* 2012, 52, 1970−1983

nonlinear optical properties of a series of bimetallic organo-iron complexes where the neutral Fe^{II}/Fe^{II} precursor formally contains a D-π-D architecture instead of D-π-A. They found that the mixed-valence Fe^{II}/Fe^{III} complex exhibits a β value twice as big as that of its neutral precursor thus giving an example of an increasing effect on β upon oxidation. There are other examples of improved hyperpolarizabilities upon oxidation (and/or reduction) in the literature. For example, one- and two-electron oxidized metalloporphyrins have shown to give higher experimental (and calculated) hyperpolarizabilities than the neutral counterparts in redox NLO-switching studies.[10] Also, recent theoretical investigations on electronic spectra and the redox-switchable second-order nonlinear optical responses of rhodium(I)-9,10-phenanthrenediimine complexes show that both one-electron oxidized and reduced complexes have higher hyperpolarizabilities than the neutral species.[11]

Because of its interesting electronic properties, thiophene-based derivatives revealed to be promising molecules for SONLO purposes.[12−15] Thus, the presence of redox-active metal centers together with a thiophene-based conjugated framework provides good opportunities for modulation of molecular NLO responses and is hence a primary justification for the study of these systems. In recent years, our group has focused in the study of intrinsic hyperpolarizabilities of η^5-monocyclopentadienyliron(II)/ruthenium(II) complexes presenting thiophene conjugated ligands coordinated to the metal center through nitrile or acetylide linkages.[16−21] Our ongoing work in this field was attracted by benzo[*c*]thiophene-based chromophores, whose unique electronic behavior originated by their low HOMO−LUMO energy gaps can be potentially on the basis of strong NLO effects.[22,23]

In this work, we report a computational study carried out by Density Functional Theory (DFT) on η^5-monocyclopentadienyliron(II) and ruthenium(II) model complexes presenting a benzo[*c*]thiophene nitrile ligand, of general formula $[MCp(P\_P)L]^+$ (M = Fe, Ru; P_P = $H_2PCH_2CH_2PH_2$; L = 5-(3-(thiophen-2-yl)benzo[*c*]thiophen-1-yl)thiophene-2-carbonitrile) in order to give a first insight on the potential use of these systems as redox-switchable SONLO materials. On the basis of the evidence found in the literature that higher hyperpolarizabilities can be achieved upon oxidation and/or reduction, our motivation in this work was to study molecules with different architectural features than the traditional D-π-A. In this case, we adopted a more likely less studied D-π-D′ feature ("off" form), for which a D-π-A′ structure ("on" form) is achieved upon oxidation and hence an expected increase on the corresponding quadratic hyperpolarizability. Because the reduction stimulus on the SONLO switching is not so well explored, we also performed this study on the present work. The calculations were performed for the complexes and free benzo[*c*]thiophene derivative ligand in order to clarify the role played by the organometallic fragment on the second-order NLO properties of these complexes.

2. METHODS

All calculations were performed at the DFT level in the gas-phase using the Gaussian 09 package.[24] As a compromise between accuracy and computational effort, we have adopted the 6-31G* basis set (for geometry optimizations) and the 6-31+G* basis set (for the calculation of hyperpolarizabilities) for C, H, N, O, and H and the LANL2DZ effective core potential basis set for S, P, Fe, and Ru.[25−28] In the case of the hyperpolarizability calculations, the LANL2DZ basis set was also augmented with a polarization function (exponents of 0.496 and 0.364) and a diffuse function (exponents of 0.0347 and 0.0298) for elements S and P, respectively.[29−31] Geometry optimizations were performed without any symmetry constrains. In all cases, the Hessian was computed to confirm the stationary points of the potential energy surfaces (PES) as true minima. In the case of the oxidized and reduced species, spin-unrestricted calculations were done. The static first hyperpolarizabilities β were calculated by using the finite field (FF) method. This methodology has been widely used because, together with electron structure methods, it can accurately compute hyperpolarizabilities.[32] The static first hyperpolarizability, β_{tot}, for all compounds was calculated by means of the analytic gradient methodology adopted in the Gaussian 09 program package by using the following equation

$$\beta_{tot} = \sqrt{\beta_x^2 + \beta_y^2 + \beta_z^2} \tag{1}$$

upon calculating the individual static components

$$\beta_i = \beta_{iii} + \frac{1}{3}\sum_{i\neq j}(\beta_{ijj} + \beta_{jij} + \beta_{jji}) \tag{2}$$

In order to obtain more insight on the description of the trends of second-order NLO response, time-dependent density functional theory (TD-DFT)[33,34] was used to compute the electronic spectra of the studied molecules applying the same theory level and basis sets used for the calculation of the hyperpolarizabilities. TD-DFT is widely used to calculate electronic spectra, and numerous attainments of this technique have been recently reviewed.[35] The first 24 lower excitation energies were computed, and the simulated absorption bands were obtained by convolution of Gaussian functions centered at the calculated excitation energies using the GaussSum[36] (version 2.2.4) software. Chemcraft[37] program (version 1.6) was used for the visualization of the computed results, including the representation of the geometries and the orbitals.

It is well known that the choice of functionals is crucial to generate reliable and accurate results. Two classes of functionals were studied in this work: two hybrid functionals, B3LYP[38,39] (Beck's three parameter functional with Lee−Yang−Parr exchange-correlations) and the CAM-B3LYP[40] (Coulomb-Atenuating Method applied to B3LYP); and a meta-hybrid generalized gradient approximation (GGA) functional, the M06 functional.[41] The B3LYP functional is one of the most widely used functionals in computational chemistry because it provides good performance in numerous energy assessments of small molecules and reproduces the geometries of smaller and larger molecules very well. Despite its success, it is well known that B3LYP can give unreliable results for determination of barriers heights, description of van der Waals interactions, isomer energy differences, and, in the case of organometallic compounds, bond energy trends and spin polarization.[42−45] In spite of these shortcomings, this functional is widely used in calculations of hyperpolarizabilities of organic and organometallic systems[46−51] and was shown to reproduce reasonably well some experimental trends.[49−51] One of the limitations of the DFT methods is the so-called "short-sightedness" of the functionals because they are based in local terms. For instance, TD-DFT calculations using popular density functionals such as B3LYP often underestimates long-range CT excitation energies, in particular for donor−acceptor substituted *push−pull* molecules.[52] Underestimation of long-range CT energetics is

a consequence of incorrect asymptotic behavior on the part of the exchange-correlation potential. This fact led to the development of the range separated functionals, where short-range HF exchange is treated using regular local functionals, like in the conventional hybrid B3LYP functional, whereas at higher interelectronic distances the long-range HF exchange is increased. The CAM-B3LYP[40] functional is one of the most recent versions of range-separated functionals, and it uses variable short-range HF exchange correlation in order to improve long-range interactions. It was found that this functional, in many cases, provides reliable results in the prediction of molecular structures, excitation energies, and hyperpolarizabilities of π-conjugated systems.[53−59] M06 is a hybrid functional for general-purpose applications and is very suitable for applications in transition metal chemistry, giving better performance than B3LYP for main-group thermochemistry, barrier heights, and noncovalent interactions.[45,60,61] Compared to B3LYP, the hybrid M06 functional presents a higher percentage of HF exchange. So far, no systematic study was executed in the performance of M06 functional for organometallic compounds, particularly in view of NLO applications, this pioneering the present study in the use of this functional.

3. RESULTS AND DISCUSSION

3.1. Geometry, Optical Data, and Hyperpolarizabilities of Benzo[*c*]thiophene Derivative Ligand and Organometallic Complexes. The optimized structures for the studied 5-(3-(thiophen-2-yl)benzo[*c*]thiophen-1-yl)-thiophene-2-carbonitrile ligand (**L**) and organometallic model complexes $[FeCp(H_2PCH_2CH_2PH_2)L]^+$ (**FeL**) and $[RuCp(H_2PCH_2CH_2PH_2)L]^+$ (**RuL**) are depicted in Figure 1 (atom

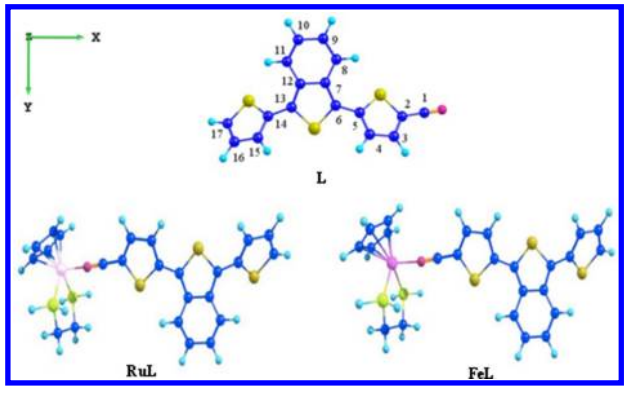

Figure 1. Representative optimized structures of **L**, **FeL**, and **RuL** using CAM-B3LYP functional (no significant differences were observed for B3LYP and M06 functionals).

numbering of the thienyl system is also included), and Table 1 shows selected bond lengths and angles. Iron and ruthenium complexes adopt typical three-legged piano-stool geometry around the metal center, where the 1,2-diphosphinoethane and thienyl ligand occupy three coordinating positions, and the η^5-cyclopentadienyl (Cp) ring occupies the remaining three positions. Upon metal coordination, bond lengths within the thienyl nitrile ligand are consistent with an increase in π-conjugation. This gives a decrease in the well-known bond-length-alternation (BLA) parameter defined as the difference between the average carbon−carbon adjacent bond lengths along a conjugated backbone. Thus, an increased contribution of the quinoidal resonance form B in the ground state upon ligand coordination is observed (Figure 2). As expected, the major effect is observed in chemical bonds close to the metal center. For instance, larger differences in the bond lengths upon coordination are observed for C1−C2 to C5−C6 (0.010−0.018 Å) than for the remaining bonds (0.001−0.008 Å). The small increase of 0.002−0.004 Å in the N≡C1 bond length upon coordination is consistent with metal-to-ligand π-backdonation interaction.

The angles and bond lengths around the metal centers and within the thienyl system for both ligand and organometallic complexes are consistent with experimental crystal data for parent iron(II) and ruthenium(II) thiophene derivatives[18,19] and other η^5-monocyclopentadienylmetal nitriles.[62−64] In general, the use of B3LYP and M06 functionals originates relatively similar bond lengths and angles, in particular, within the conjugate thienyl nitrile framework. CAM-B3LYP provides shorter bond lengths in the case of multiple bonds and stretched bond lengths for single bonds. Thus, larger BLAs are observed with CAM-B3LYP. Considering the calculated data for the molecules studied in this work, this functional reproduces more successfully and with better accuracy the experimental data reported for the parent iron(II) and ruthenium(II) thiophene derivatives.[18,19] For long conjugated systems, CAM-B3LYP functional has proven, in fact, to lead to more accurate values of BLA when compared to the ones obtained with B3LYP.[55,65,66]

After the geometry optimization, the static first hyperpolarizabilities for **L**, **FeL**, and **RuL** were calculated, and relevant results are shown in Table 2.

The β_{tot} values of the three molecules are functional-dependent, in particular for organometallic complexes. Except for B3LYP, coordination of the ligand to organometallic moieties enhances the second-order NLO properties, particularly using CAM-B3LYP. On the basis of the complex sum-over-states expression, Oudar and Chemla established a link between the molecular hyperpolarizability and low energy charge transfer transition through the two-level model (TLM)[67]

$$\beta \propto \frac{\Delta\mu_{eg} f_{eg}}{E_{eg}^3} \tag{1}$$

where $\Delta\mu_{eg}$ is the difference between the dipole moments of the ground (g) and the excited (e) state, f_{eg} is the oscillator strength, and E_{eg} is the transition energy. Those factors ($\Delta\mu_{eg}$, f_{eg}, and E_{eg}) are all closely related and are controlled by the electronic properties of the molecules. An optimal combination of those factors will provide a higher β value. This model is a good approximation for estimate the second-order polarizabilities of donor/acceptor dipolar NLO chromophores and assumes that only one excited state is coupled strongly enough to the ground state by the applied electric field, and only one component of the β tensor dominates the NLO response (i.e., a unidirectional charge-transfer transition). For **L**, **FeL**, and **RuL**, β_{tot} is clearly dominated by the β_{xxx} tensor component (along the charge transfer axis; see Supporting Information). Thus, an analysis of the results according to the TLM seems to be reasonable for these molecules. Besides, to get more insight about the second-order NLO response of these molecules, we have performed TD-DFT calculations. The relevant excitation energies, oscillator strengths and orbital transitions have been listed in Table 3.

Table 1. Selected Calculated Structural Data for L, FeL, and RuL[a]

	B3LYP			CAM-B3LYP			M06		
	L	**FeL**	**RuL**	**L**	**FeL**	**RuL**	**L**	**FeL**	**RuL**
Bond Lengths (Å)									
Cp[b]–M	–	1.763	1.892	–	1.738	1.867	–	1.673	1.845
M–N	–	1.925	2.069	–	1.933	2.076	–	1.899	2.087
M–P[c]	–	2.334	2.423	–	2.325	2.415	–	2.279	2.418
N–C1	1.166	1.170	1.170	1.158	1.160	1.160	1.166	1.170	1.169
C1–C2	1.410	1.392	1.393	1.415	1.399	1.400	1.409	1.391	1.392
BLA[d]	0.050	0.036	0.038	0.065	0.052	0.053	0.050	0.038	0.038
Bond Angles (deg)									
Cp[b]–M–N	–	125.3	125.8	–	124.5	125.9	–	126.5	128.7
M–N–C1	–	175.9	173.5	–	176.3	174.2	–	178.4	177.0
P1–M–P2	–	85.2	82.6	–	85.2	82.7	–	85.9	82.3
N–C1–C2	179.8	179.7	179.9	179.9	179.7	179.8	179.9	178.4	178.8
D_h[e](C4–C5–C6–C7)	156.7	169.2	168.2	149.8	163.8	162.4	158.2	167.4	166.5
D_h[e](C12–C13–C14–C15)	150.4	152.0	151.9	144.8	146.4	146.2	151.1	152.9	152.6

[a]Additional structural data is shown in the Supporting Information. [b]η^5-C_5H_5 centroid. [c]Average M-P1/P2 bond lengths (no significant changes were observed between M–P1 and M–P2 bond lengths). [d]Bond Length Alternation. [e]Dihedral angle.

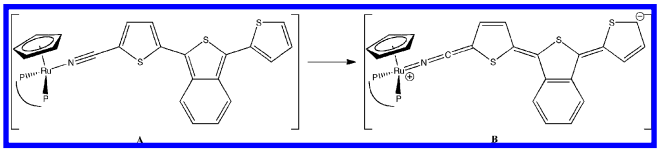

Figure 2. Resonance forms $[MCp(H_2PCH_2CH_2PH_2)L]^+$.

Table 2. β_{tot} for L, FeL, and RuL[a]

	β_{tot} (10^{-30} esu)		
	B3LYP	CAM-B3LYP	M06
L	39.94	30.06	36.79
FeL	33.54	113.64	49.43
RuL	31.52	105.78	57.07

[a]The corresponding β tensor components are shown in the Supporting Information.

The main optical feature for all molecules is the presence of an intense electronic transition (ET) attributed to HOMO→LUMO charge transfer. Our TD-DFT calculation predicts electronic transitions at low energy and with substantial oscillator strength in the gas phase, which are the key for second-order nonlinear optical properties. Our experimental results of UV–vis spectra for **L**, $[FeCp(DPPE)L]^+$ (related to the model **FeL** complex), and $[RuCp(DPPE)L]^+$ (related to the model **RuL** complex) reveal a very intense absorption band at 456, 487, and 460 nm, respectively, in dichloromethane.[68] Despite that all the functionals predict a red-shift of this band upon ligand coordination to the iron and ruthenium organometallic moieties, in accordance to the experimental data, B3LYP and M06 functionals underestimate the low-lying electronic transition energies for these compounds. However, the CAM-B3LYP functional gives optical transition energies very close to the experimental values, in particular for **FeL**, thus reproducing the experimental data more successfully and with better accuracy.

The frontier molecular orbitals for **L**, **FeL**, and **RuL** obtained using CAM-B3LYP are depicted in Figure 3 (no significant differences were found for the same orbitals using B3LYP and M06 functionals).

HOMOs and LUMOs for all molecules are relatively spread over the ligand with only a small contribution of the metal atom in the case of organometallic complexes. An analysis of the electronic transition in terms of the contributions of groups of

Table 3. Relevant TD-DFT Results for L, FeL, and RuL

Comp.	Functional	λ_{eg}[a] (nm)	E_{eg}[b] (eV)	f_{eg}[c]	Major contributions[d]	Character of the CT[e]
L	B3LYP	512	2.426	0.6021	H→L (100%)	BcT (50), T2 (50) → NC-T1 (100)
	CAM-B3LYP	431	2.883	0.6132	H→L (97%)	BcT (55), T2 (45) → NC-T1 (100)
	M06	508	2.445	0.5764	H→L (100%)	BcT (56), T2 (44) → NC-T1 (100)
FeL	B3LYP	565	2.196	0.9501	H→L (98%)	BcT (33), T2 (47), OM (20) → NC-T1 (100)
	CAM-B3LYP	487	2.499	0.7089	H→L (77%)	BcT (52), T2 (43), OM (5) → NC-T1 (100)
	M06	558	2.225	0.9268	H→L (100%)	BcT (33), T2 (44), OM (23) → NC-T1 (100)
RuL	B3LYP	565	2.196	0.9867	H→L (100%)	BcT (35), T2 (47), OM (18) → NC-T1 (100)
	CAM-B3LYP	486	2.553	0.9636	H→L (96%)	BcT (56), T2 (41), OM (3) → NC-T1 (100)
	M06	557	2.231	0.9402	H→L (99%)	BcT (39), T2 (44), OM (17) → NC-T1 (100)

[a]Absorption wavelength of the main transitions. [b]Energy of the transitions. [c]Oscillator strength. [d]H-HOMO, L-LUMO. [e]Based on the represented fragments (overall % of the charge transfer in parentheses). T: Tiophene rings (T1-close to NC; T2-second ring). BcT: Benzo[*c*]thiophene group. OM: Organometallic fragment (M+Cp+Phosphine coligand).

dx.doi.org/10.1021/ci300226t | J. Chem. Inf. Model. 2012, 52, 1970–1983

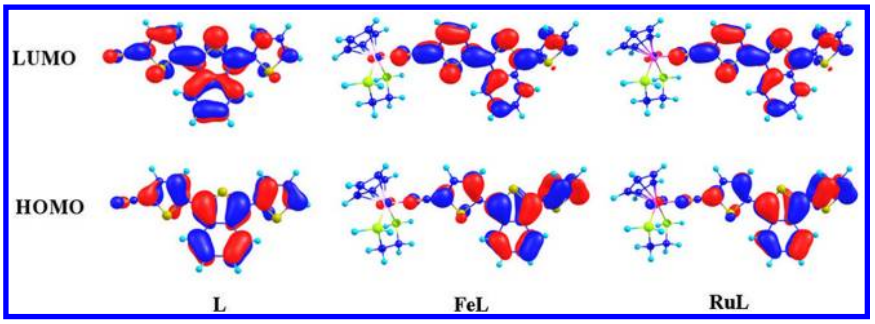

Figure 3. Molecular orbitals of **L**, **FeL**, and **RuL** involved in the dominant optical transitions.

Table 4. Selected Calculated Structural Data[a] for L^{ox}, FeL^{ox}, and RuL^{ox}

	B3LYP			CAM-B3LYP			M06		
	L^{ox}	FeL^{ox}	RuL^{ox}	L^{ox}	FeL^{ox}	RuL^{ox}	L^{ox}	FeL^{ox}	RuL^{ox}
Bond Lengths (Å)									
Cp^b–M	–	1.767	1.907	–	1.741	1.875	–	1.688	1.865
M–N	–	1.878	2.028	–	1.909	2.053	–	1.853	2.043
M–P[c]	–	2.347	2.437	–	2.331	2.422	–	2.289	2.423
N–C1	1.165	1.173	1.173	1.158	1.159	1.160	1.165	1.174	1.172
C1–C2	1.410	1.394	1.395	1.414	1.409	1.408	1.410	1.391	1.394
BLA[d]	0.015	0.009	0.010	0.020	0.016	0.016	0.015	0.009	0.010
Bond Angles (deg)									
Cp^b–M–N	–	124.0	125.7	–	123.6	125.3	–	125.7	127.9
M–N–C1	–	173.4	172.5	–	173.4	172.3	–	175.2	174.2
P1–M–P2	–	84.6	81.8	–	84.8	82.2	–	85.2	81.8
N–C1–C2	179.8	178.3	178.6	179.8	178.1	178.2	179.8	179.2	179.6
D_h[e](C4–C5–C6–C7)	171.0	172.8	173.7	172.7	171.6	172.7	171.5	177.5	177.7
D_h[e](C12–C13–C14–C15)	169.1	169.7	169.5	171.3	174.2	174.2	169.6	170.1	170.7

[a]Additional structural data is shown in Supporting Information. [b]η^5-C_5H_5 centroid. [c]Average M-P1/P2 bond lengths (no significant changes were observed between M-P1 and M-P2 bond lengths). [d]Bond Length Alternation. [e]Dihedral angle.

Table 5. Selected Calculated Structural Data[a] for L^{red}, FeL^{red}, and RuL^{red}

	B3LYP			CAM-B3LYP			M06		
	L^{red}	FeL^{red}	RuL^{red}	L^{red}	FeL^{red}	RuL^{red}	L^{red}	FeL^{red}	RuL^{red}
Bond Lengths (Å)									
Cp^b–M	–	1.771	1.903	–	1.741	1.87	–	1.674	1.849
M–N	–	1.957	2.120	–	1.951	2.109	–	1.967	2.156
M–P[c]	–	2.319	2.403	–	2.316	2.401	–	2.267	2.401
N–C1	1.173	1.191	1.193	1.165	1.183	1.185	1.175	1.192	1.194
C1–C2	1.397	1.361	1.360	1.400	1.357	1.356	1.396	1.356	1.356
BLA[d]	0.016	0.003	0.003	0.020	0.000	0.000	0.016	0.001	0.001
Bond Angles (deg)									
Cp^b–M–N	–	124.2	124.6	–	124.9	125.5	–	124.8	125.6
M–N–C1	–	147.8	140.7	–	149.2	141.9	–	136.5	129.7
P1–M–P2	–	85.8	82.9	–	85.7	82.8	–	86.2	82.2
N–C1–C2	180.0	177.8	177.9	179.9	177.9	178.2	179.8	176.0	176.2
D_h[e](C4–C5–C6–C7)	180.0	179.0	179.5	180.0	179.5	179.6	180.0	178.8	179.4
D_h[e](C12–C13–C14–C15)	180.0	170.3	171.3	180.0	173.2	172.9	180.0	171.9	176.3

[a]Additional structural data is shown in Supporting Information. [b]η^5-C_5H_5 centroid: [c]Average M-P1/P2 bond lengths (no significant changes were observed between M-P1 and M-P2 bond lengths); [d]Bond Length Alternation; [e]Dihedral angle

atoms involved using GaussSum software[36] (Table 3) show that for **L** the charge transfer associated to HOMO→LUMO mainly arises from the donor thienyl and benzo[*c*]thiophene rings to the acceptor thienyl-nitrile unit. The character of the main electronic transition for **FeL** and **RuL** is also dominated by a charge transfer mainly within the ligand fragment (ILCT) with some contribution of metal-to-ligand charge transfer (MLCT). The overall results show that thienyl ring farthest from the NC group, and the benzo[*c*]thiophene moiety behaves as a donor in these molecules and agrees to the fact that thiophene rings can behave as a donor in π-conjugated systems presenting electron-withdrawing groups,[69] which is the case with our ligand. Considering the well-known electron donor character of the organometallic fragments, these molecules can be viewed as

dx.doi.org/10.1021/ci300226t | J. Chem. Inf. Model. 2012, 52, 1970−1983

having a structure of type D-π-D′. CAM-B3LYP predicts only small contributions of a MLCT character to the overall electronic transition (5% for **FeL** and 3% for **RuL**), whereas B3LYP and M06 functionals predicts larger contributions (20−23% for **FeL** and 17−18% for **RuL**). Because a red-shift of this electronic transition is observed upon ligand coordination, an increase of the corresponding hyperpolarizabilities is expected, according to the TLM. CAM-B3LYP clearly predicts an increase in β_{tot}, as expected, whereas B3LYP and M06 functionals give moderate changes on hyperpolarizabilities upon ligand coordination (Table 2). Probably the different contribution of a MLCT character to the overall electronic transition predicted by B3LYP and M06 functionals (up to 23%) when compared to that predicted by CAM-B3LYP (3−5%) could explain the changes on β_{tot} upon ligand coordination. In fact, an enhanced contribution of a MLCT (with variation of the dipole moment against to that observed in the main ILCT process) might lead to a hampering effect on β_{tot} due to less change on the dipolar moment upon excitation.

Our recent experimental results of quadratic hyperpolarizabilities measured at 1500 nm by HRS method in chloroform for $[FeCp(DPPE)L]^+$ (related to the model **FeL** complex) and $[RuCp(DPPE)L]^+$ (related to the model **RuL** complex) show β_0 values (β corrected for resonance enhancement using the two-level model) of 87×10^{-30} esu and 80×10^{-30} esu, respectively.[68] From Table 2 it can be seen that, in general, the CAM-B3LYP functional seems to better reproduce the experimental hyperpolarizabilities. This fact, together with the results obtained in structural and optical studies (see above) suggests that the CAM-B3LYP functional predicts experimental data of the molecules studied in this work with more reliability.

3.2. Redox Switching of Second-Order NLO Responses. We investigated the possibility of second-order NLO switching of **L**, **FeL**, and **RuL** by redox means. Unrestricted calculations of the one-electron-oxidized ($\mathbf{L}^{ox}$, $\mathbf{FeL}^{ox}$, and $\mathbf{RuL}^{ox}$) and one-electron-reduced ($\mathbf{L}^{red}$, $\mathbf{FeL}^{red}$, and $\mathbf{RuL}^{red}$) species were performed. First, geometries were optimized followed by the calculations of the hyperpolarizabilities. Structural changes are observed in all species upon oxidation/reduction (Tables 4 and 5).

Comparison of Tables 1 and 4 show the following general trends upon oxidation: (i) slight lengthening of the Cp−M and M−P bonds; (ii) strong shortening of the M−NC bond; (iii) minimal changes on N≡C bond length for ligands and complexes; (iv) decrease in angles around the metal center, in particular for M−N≡C1; (v) decrease in the N≡C1−C2 bond angle (except for complexes with M06 functionals); and (vi) increased planarity within the conjugated thienyl system, in particular for organometallic complexes. The lengthening of the Cp−M and M−P bonds upon oxidation are consistent with crystal data of piano-stool Fe(III) and Ru(III) complexes.[70−72] The improved planarity within the conjugated thienyl system upon oxidation (dihedral angles between thienyl rings for oxidized species close to 180°, in comparison with nonoxidized species) is accompanied by the expected decrease in BLA parameter (Table 4). Thus, an enhanced contribution of the quinoidal resonance forms (Figure 2) in the ground state upon oxidation is observed (some deviation of N≡C1−C2 from linearity is consistent with this observation). The major changes in the bond lengths within the conjugated thienyl system, responsible for this behavior, are observed in the two thienyl rings farthest from the metal center. Thus, a more effective conjugation length is observed upon oxidation.

The following general trends are observed upon reduction by comparison of Tables 1 and 5: (i) lengthening of Cp−M and shortening of M−P bonds; (ii) strong lengthening of M−NC bond, in particular for ruthenium complex; (iii) increase in N≡C bond length, in particular for organometallic complexes; (iv) strong decrease in M−N≡C1 angles, in particular for the Ru complex; and (v) increased planarity within the conjugated thienyl system, in particular for organometallic complexes. As was observed upon oxidation, the improved planarity within the conjugated thienyl system upon reduction is accompanied by the expected decrease in BLA parameter (Table 4). The effect is now somewhat enhanced. In fact, the dihedral angles between thienyl rings for reduced species are even closer to 180° in comparison with oxidized species, and the BLA parameter is almost zero. Thus, for $\mathbf{FeL}^{red}$ and $\mathbf{RuL}^{red}$ almost an equal contribution of the aromatic/quinoidal resonance forms are achieved in ground state (Figure 2). The major changes in bond lengths within the conjugated thienyl system, responsible for this behavior, are observed in the two thienyl rings closest of the metal center.

The overall results show that most significant structural changes upon the oxidation/reduction process are observed on organometallic complexes. Major differences between oxidation vs reduction are observed on (i) M−NC bond length: oxidation originates strong shortening, whereas reduction provides strong lengthening; (ii) N≡C bond: both increase bond length, but the reduction process results in an enhanced effect; (iii) M−N≡C1 angle: both decrease the bond angle, but the reduction process originates a stronger effect; (iv) planarity within the conjugated thienyl system: both originate enhanced planarity, but an improved effect is observed upon reduction. As is well known, the molecular electrostatic potentials (MEPs) are highly informative concerning the nuclear and electronic charge distribution of a given molecule. To further investigate the influence of redox stimulus on the electronic charge distribution, the MEP maps of **FeL**, $\mathbf{FeL}^{ox}$, and $\mathbf{FeL}^{red}$ are given in Figure 4.

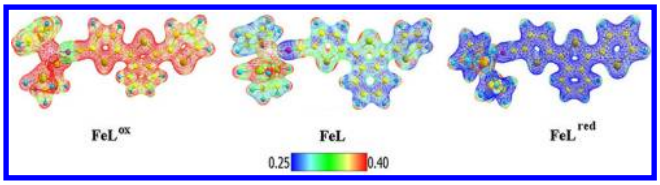

Figure 4. Molecular electrostatic potential (MEP) maps distributions for $\mathbf{FeL}^{ox}$, **FeL**, and $\mathbf{FeL}^{red}$ using CAM-B3LYP.

The results show that **FeL** has less positive charge densities (blue region) mainly located in the thienyl ligand and more positive charge densities in the organometallic fragment, in particular on metal and phosphorus atoms. Upon one-electron oxidation, the entire molecule becomes more positive, and the major changes are verified in the thienyl ligand. Upon one-electron reduction, the entire molecule becomes less positive, and the major changes are verified in the organometallic fragment. Thus, both oxidation and reduction lead to a more homogeneous charge density distribution within the molecule, which seems to agree with the enhanced conjugation length determined by BLA analysis.

Considering the different studied functionals, the same general observations as those obtained in the nonoxidized/reduced species **L**, **FeL**, and **RuL** are observed in the oxidized/

Table 6. β_{tot}[a] and Relevant TD-DFT Results for L^{ox}, FeL^{ox}, and RuL^{ox}

Comp.	Functional	λ_{eg}[b] (nm)	E_{eg}[c] (eV)	f_{eg}[d]	Major contributions[e]	β_{tot} (10^{-30} esu)	$\beta_{tot}^{ox}/\beta_{tot}$
L^{ox}	B3LYP	582	2.13	0.2218	βH-1→βL (47%); βH→βL (26%)	41.93	1.04
		568	2.18	0.3603	βH-1→βL (33%); βH→βL (33%)		
	CAM-B3LYP	547	2.27	0.6261	βH→βL (63%); αH→αL (14%)	53.38	1.77
	M06	575	2.16	0.3836	βH→βL (46%); βH-1→βL (20%)	44.32	1.20
FeL^{ox}	B3LYP	1492	0.83	0.3207	βH→βL (91%)	7268.15	216.70
		863	1.44	0.2410	αH→αL (72%)		
	CAM-B3LYP	633	1.96	0.6068	βH→βL (57%)	622.67	5.47
		546	2.28	0.2651	βH-2→βL (48%)		
	M06	1365	0.91	0.2801	βH→βL (85%)	4090.95	82.76
		842	1.48	0.2811	αH→αL (62%)		
		583	2.13	0.2955	βH-3→βL (27%); αH→αL (17%)		
RuL^{ox}	B3LYP	1222	1.02	0.2121	βH→βL (86%)	2120.27	67.27
		852	1.46	0.3876	αH→αL (63%)		
		618	2.01	0.2203	αH-1→αL (31%); βH-3→βL (21%)		
	CAM-B3LYP	675	1.84	0.6324	βH→βL (61%)	874.41	8.27
		546	2.28	0.3044	βH-3→βL (53%)		
	M06	1202	1.03	0.2114	βH→βL (87%)	2134.89	37.41
		850	1.46	0.3401	αH→αL (53%)		
		615	2.02	0.2423	αH→αL (29%); βH-3→βL (22%)		

[a]The corresponding β tensor components are shown in the Supporting Information. [b]Absorption wavelength of the main transitions. [c]Energy of the transitions. [d]Oscillator strength. [e]H-HOMO, L-LUMO.

Table 7. β_{tot}[a] and Relevant TD-DFT Results for L^{red}, FeL^{red}, and RuL^{red}

Comp.	Functional	λ_{eg}[b] (nm)	E_{eg}[c] (eV)	f_{eg}[d]	Major contributions[e]	β_{tot} (10^{-30} esu)	$\beta_{tot}^{red}/\beta_{tot}$
L^{red}	B3LYP	663	1.87	0.4306	αH→αL (62%); βH→βL (21%)	45.78	1.15
	CAM-B3LYP	635	1.96	0.4883	αH→αL (67%); βH→βL (12%)	92.69	3.08
	M06	666	1.86	0.4321	αH→αL+2 (66%); βH→βL (19%)	58.18	1.58
FeL^{red}	B3LYP	815	1.52	0.1988	βH→βL (36%); αH→αL+1 (22%)	582.14	17.36
		547	2.27	0.1903	αH-1→αL+1 (21%); βH→βL+2 (11%)		
	CAM-B3LYP	608	2.04	0.5255	βH→βL (33%); αH→αL+2 (17%)	99.11	0.87
		479	2.59	0.2827	αH-1→αL+2 (10%); βH→βL+3 (11%)		
	M06	693	1.79	0.1974	βH→βL (19%); αH→αL+2 (54%)	336.85	6.81
RuL^{red}	B3LYP	785	1.58	0.3333	βH→βL (49%); αH→αL (19%)	499.44	15.85
		631	1.97	0.2114	αH→αL+2 (64%); βH→βL (13%)		
		606	2.05	0.3009	αH→αL+3 (28%); βH→βL (14%)		
	CAM-B3LYP	617	2.01	0.7021	βH→βL (54%); αH→αL (21%)	45.06	0.42
	M06	755	1.64	0.2580	βH→βL (42%); αH→αL (26%)	278.87	4.89
		607	2.05	0.2181	αH→αL+5 (51%); βH→βL (15%)		

[a]The corresponding β tensor components are shown in the Supporting Information. [b]Absorption wavelength of the main transitions. [c]Energy of the transitions. [d]Oscillator strength. [e]H-HOMO, L-LUMO.

reduced counterparts. Thus, B3LYP and M06 functionals give similar bond lengths and angles within the thienyl nitrile framework. In addition, CAM-B3LYP provides somewhat larger BLAs than those produced by B3LYP and M06, with the exception of the organometallic reduced species. In the case of chemical bonds involving metal atoms, the same general trends are also observed: (1) major differences are obtained for Fe species, (2) B3LYP and CAM-B3LYP predict closer bond lengths and angles values, and (3) M06 gives higher angles and shorter bond lengths when compared to the B3LYP and CAM-B3LYP functionals.

The relevant results for the static first hyperpolarizabilities and TD-DFT calculation for both oxidized and reduced species are listed in Tables 6 and 7.

The results show that β_{tot} values (a) are dominated by β_{xxx} tensor (the only exception is **RuL**^{red} using CAM-B3LYP functional), (b) are functional-dependent, and (c) indicate a clear dependence on NLO responses from the redox stimulus. In particular, the oxidation of organometallic complexes significantly enhances second-order hyperpolarizabilities: the β_{tot} of **FeL**^{ox} enhances up to 217 times relatively to **FeL** and β_{tot} of **RuL**^{ox} enhances up to 67 times relatively to **RuL**, depending on the used functional. Instead, the oxidation of **L** gives moderate enhancing effect on β_{tot}. Reduction of the studied molecules originates some subtle results. As in the oxidation process, the reduction of **L** leads to a moderate enhancing effect on β_{tot}, although the increase of β_{tot} is now slightly higher. For organometallic complexes, the use of different functionals

dx.doi.org/10.1021/ci300226t | J. Chem. Inf. Model. 2012, 52, 1970−1983

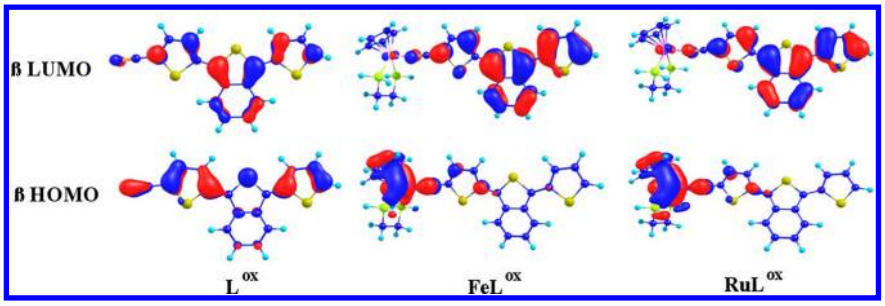

Figure 5. The molecular orbitals of $\mathbf{L}^{ox}$, $\mathbf{FeL}^{ox}$, and $\mathbf{RuL}^{ox}$ involved in the dominant optical transitions.

originates contradictory results. By using B3LYP and M06 functionals, an increase in β_{tot} is observed, although more moderate than observed with the oxidation process: β_{tot} of $\mathbf{FeL}^{red}$ and $\mathbf{RuL}^{red}$ enhances up to 16−17 times relatively to **FeL** and **RuL**, depending on the functional used. However, by using CAM-B3LYP, β_{tot} decreases upon reduction, in particular for the ruthenium complex. The β_{tot} of oxidized and reduced species, in particular for organometallic complexes, using B3LYP and M06 functionals seem to be not reasonable. In fact, these values appear to be largely overestimated because they arise from the unexpected and unrealistic low-energy charge transfer transitions, especially for oxidized species (vide infra).

The main optical feature for all oxidized molecules is the presence of low energy electronic transitions attributed to HOMOs→LUMOs charge transfer. The significant molecular orbitals for $\mathbf{L}^{ox}$, $\mathbf{FeL}^{ox}$, and $\mathbf{RuL}^{ox}$, obtained using CAM-B3LYP, are depicted in Figure 5. No significant differences were found for the same orbitals using B3LYP and M06 functionals.

For $\mathbf{L}^{ox}$, the charge transfer associated to the βHOMO→βLUMO transition mainly arises from the side thienyl rings to the benzo[*c*]thienyl group. For oxidized organometallic complexes, it is clearly seen that βHOMOs are located in the organometallic moiety and βLUMOs are spread over the ligand. Therefore, βHOMO→βLUMOs transitions can be assigned to MLCT. As discussed above, HOMO→LUMO excitations of **FeL** and **RuL** were assigned as an ILCT because both HOMO and LUMO clearly have ligand character (Figure 3). Consequently, compared to the parent transition in $\mathbf{L}^{ox}$ and nonoxidized organometallic complexes, βHOMO→βLUMO transition of $\mathbf{FeL}^{ox}$ and $\mathbf{RuL}^{ox}$ can lead to an effective charge transfer from the organometallic moiety to the ligand. This feature is supported by the almost linear M−N≡C1−C2 geometry, which favors metal-to-ligand π-backdonation interaction and a more effective conjugation length observed upon oxidation. In fact, the most significant optical changes upon one-electron oxidation are a strong red shift of the main electronic transitions and a decrease in the corresponding oscillator strength (Table 6). Besides, additional optical transitions at lower energies are observed in organometallic complexes, compared to the ones presented by $\mathbf{L}^{ox}$. As an example, the calculated optical spectra using CAM-B3LYP for $\mathbf{L}^{ox}$, $\mathbf{FeL}^{ox}$, $\mathbf{RuL}^{ox}$, and **RuL** depicted in Figures 6 and 7 show this behavior.

According to the TLM, the overall effect should lead to an increase in the NLO response upon oxidation for all molecules, in particular for organometallic complexes. The calculated β_{tot} values are in agreement with those expected trends (Table 6). For instance, using CAM-B3LYP, the transition energies of major molecular orbital transitions decrease in the following order: $\mathbf{L}^{ox} \gg \mathbf{FeL}^{ox} > \mathbf{RuL}^{ox}$, and no significant differences on the corresponding oscillator strength is observed. Thus, β_{tot} increases as follows: $\mathbf{L}^{ox} \ll \mathbf{FeL}^{ox} < \mathbf{RuL}^{ox}$. According to CAM-B3LYP results, the ruthenium complex seems to be the better candidate for NLO switching through an oxidation stimulus. In

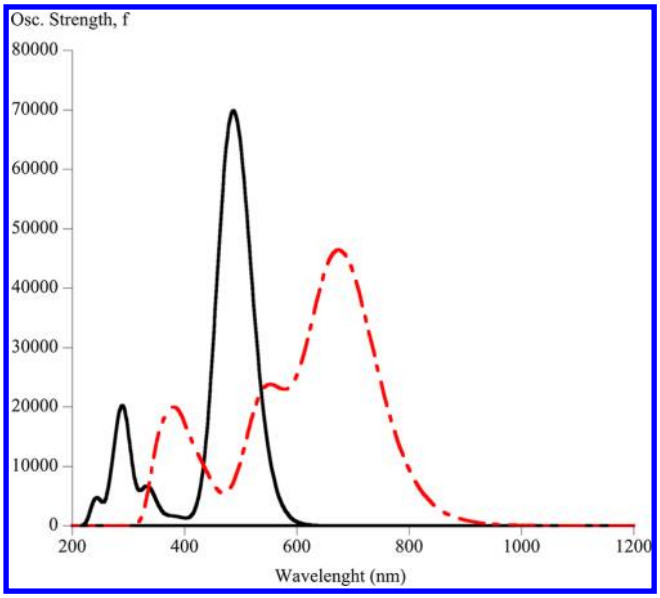

Figure 6. Calculated optical spectra for **RuL** (−) and $\mathbf{RuL}^{ox}$ (−•−).

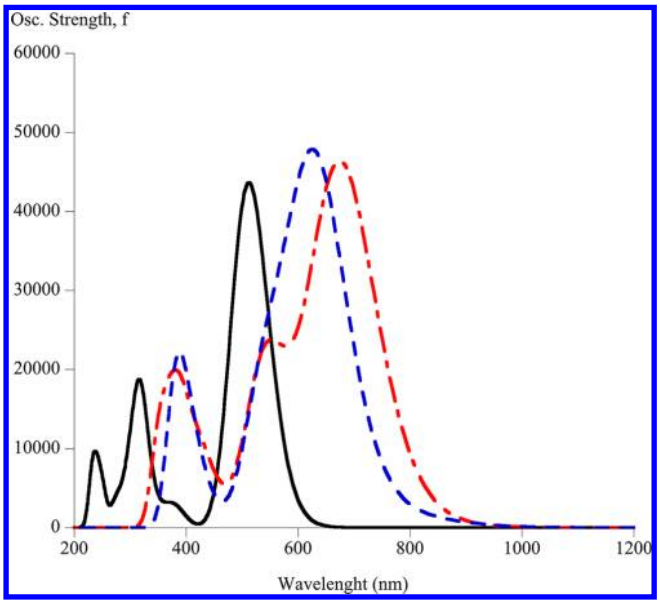

Figure 7. Calculated optical spectra for $\mathbf{L}^{ox}$ (−), $\mathbf{FeL}^{ox}$ (−), and $\mathbf{RuL}^{ox}$ (−•−).

dx.doi.org/10.1021/ci300226t | *J. Chem. Inf. Model.* 2012, 52, 1970−1983

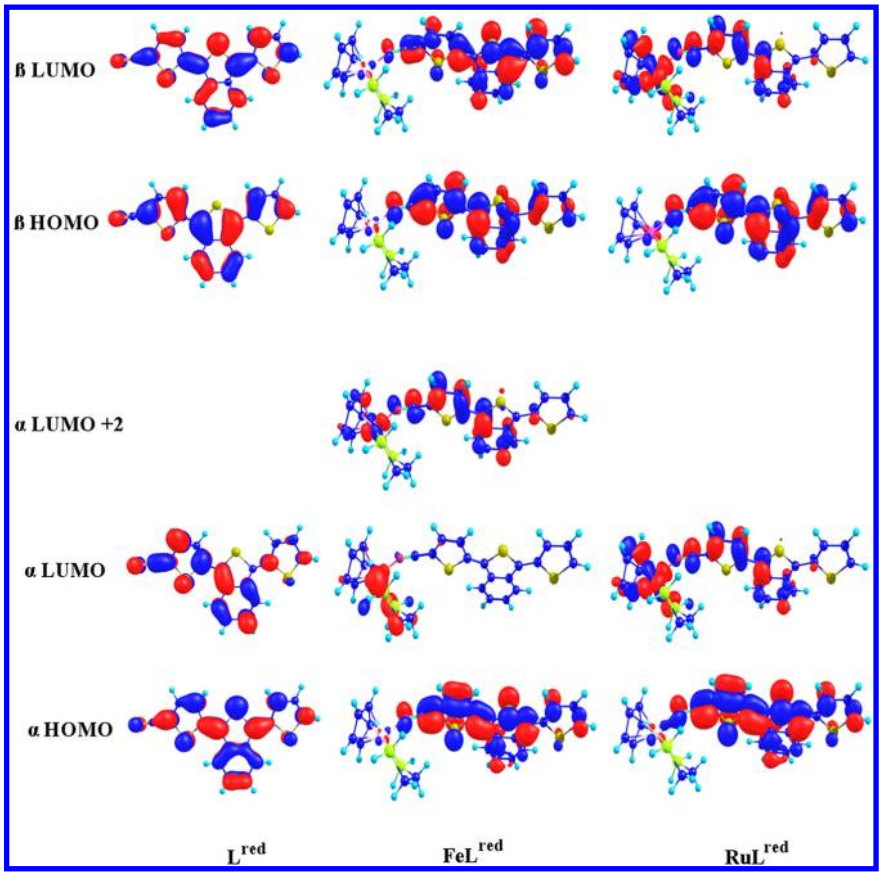

Figure 8. Molecular orbitals of $\mathbf{L}^{red}$, $\mathbf{FeL}^{red}$, and $\mathbf{RuL}^{red}$ involved in the dominant optical transitions using CAM-B3LYP.

fact, β_{tot} of $\mathbf{RuL}^{ox}$ enhances 8.27 times relative to **RuL**, whereas β_{tot} of $\mathbf{FeL}^{ox}$ enhances 5.47 times relative to **FeL**. Nevertheless, B3LYP and M06 give opposite relative trend results, i.e., the enhancing effect on the iron compound upon oxidation is higher than the predicted in ruthenium complex. In addition, these functionals predict significant enhancement of β_{tot} upon oxidation compared with that obtained with CAM-B3LYP. As mentioned above, these values seem to be overestimated because they arise from the unexpected very low energies of βHOMO→βLUMO transition in the NIR region. It is well known that the B3LYP functional, with low percentage of HF orbital exchange, can overestimate molecular hyperpolarizabilities, in particular for large conjugated molecules. The reason is related to the self-interaction error in the exchange part of the density functional,[73−75] which is responsible for overdelocalization of the electron density. This result in incorrect screening of the external electric field[76] and incorrect description of the charge transfer processes[77] often lead to an underestimation of the energies of excitations with a long-range spatial extent.[35,52] The M06 functional, more suitable for applications in transition metal chemistry,[45] has a fixed percentage of HF exchange (as B3LYP), and similar deviations than the observed using B3LYP functional could be observed. In the case of oxidized complexes, βHOMO→βLUMO transitions can be clearly assigned to MLCT. Thus, a charge transfer from a low-energy occupied orbital (centered in the organometallic fragment) to a virtual unoccupied orbital located in another part of the molecule (thienyl moiety) results in a charge separation. Therefore, a Coulombic interaction within this charge-separated excited stated should be taken into account, in terms of an attractive 1/R dependence. CAM-B3LYP, which contains long-range corrected effects using the Coulomb-attenuating method, can overcome (at least partially) this problem because it corrects the potential energy curves of the charge transfer state along the orbital separation coordinate resulting in a better description of the mentioned excited state and hence a better estimation of the charge transfer energy. Thus, the hyperpolarizabilities obtained with B3LYP and M06 functionals are consistent with the underestimation of the charge transfer energies and are by far an overestimation of such property for the organometallic oxidized molecules.

The fact that oxidation leads to improved hyperpolarizabilities should be commented on here. Most of the metal−organic compounds studied for SONLO switching are typically push−pull systems in which the metal center acts as an electron-donor group in a dipolar donor/conjugated bridge/acceptor (D-π-A) structure. According to the well-known type I switching mechanism, upon oxidation the donor becomes a competing acceptor moiety (A′) thus leading to lower hyperpolarizability.[5] In the case of the molecules studied in this work, with a more likely less studied D-π-D′ feature, the oxidation leads to the achievement of a D-π-A′ structure and hence an expected increase on the corresponding quadratic hyperpolarizability. The electronic behavior of the thiophene ring farthest from the NC group, and benzo[*c*]thiophene moiety is reversed upon oxidation as can be seen clearly by the analysis of the orbitals depicted in Figure 5, i.e., behave as a donor in nonoxidized species (**FeL** and **RuL**) and electron-acceptor in the oxidized form. Thus, the charge transfer in oxidized molecules resembles the behavior found in the classic picture of the metal as donor and a ligand with an acceptor moiety. Some examples of improved hyperpolarizabilities upon

oxidation are found in the literature. For instance, Weyland et al. have investigated the effect of oxidation state on the second-order nonlinear optical properties of a series of bimetallic organo-iron complexes where a neutral Fe^{II}/Fe^{II} precursor formally contains a D-π-D architecture instead of D-π-A.[9] They found that the mixed-valence Fe^{II}/Fe^{III} complex exhibits a β value twice as big as that of its neutral precursor. In addition, NLO-switching studies on metalloporphyrins[10] and rhodium(I)-9,10-phenanthrenediimine complexes[11] show that oxidized species present higher hyperpolarizabilities than their neutral counterparts. Considering rhodium(I)-9,10-phenanthrenediimine complexes, changes in the CT feature were observed, in which the donor metal fragment plays an improved role in the hyperpolarizabilities of the oxidized species. The same general behavior was found upon oxidation of **FeL** and **RuL**.

Considering the reduction stimulus, the main optical feature for reduced molecules is the presence of a low energy electronic transition, mainly attributed to HOMOs→LUMOs charge transfer. For $\mathbf{FeL}^{red}$, additional contribution of a αH→αL+1 or αH→αL+2 (depending on the used functional) is also observed. For organometallic complexes, further electronic transitions at higher energies are observed with almost similar oscillator strength than for HOMOs→LUMOs. The significant molecular orbitals for $\mathbf{L}^{red}$, $\mathbf{FeL}^{red}$, and $\mathbf{RuL}^{red}$ obtained using CAM-B3LYP are depicted in Figure 8. No significant differences were found for the same orbitals using B3LYP and M06 functionals.

According to the orbital densities, the lower-energy electronic transition of reduced organometallic complexes has contributions of ILCT and LMCT. Thus, it is primarily the ligand that is reduced, so that its donor strength is enhanced compared to the nonreduced species, leading to a charge transfer contribution to the organometallic moieties that becomes an acceptor. The changing of the structural feature of the molecules studied in this work, in which the organometallic moiety becomes an electron acceptor, reveals their inadequacy for an efficient NLO-switching by reduction means because they are known as strong electron donors. In fact, improved hyperpolarizabilities are expected when these organometallic moieties behaves as a donors and are coupled with strong electron acceptors as was observed in largely studied D-π-A molecular feature complexes.[17,64,78−82] This behavior can be emphasized if we consider the study of the redox-switchable second-order nonlinear optical responses of rhodium(I)-9,10-phenanthrenediimine[11] and noninnocent ruthenium[83] complexes, for which the increase in second-order NLO response upon reduction has been attributed to MLCT transitions. Thus, significant changes are not expected on the quadratic hyperpolarizabilities of the complexes studied in this work upon reduction when compared to those observed upon oxidation in which the organometallic moiety behaves as a donor. In fact, Table 7 shows that the changes on the calculated quadratic hyperpolarizabilities upon reduction are significantly lower than that observed upon oxidation (Table 6).

Compared to **FeL** and **RuL**, a red-shift of the main optical transitions and a decrease in the corresponding oscillator strength is observed in reduced species. As was observed with oxidation stimulus, CAM-B3LYP functional gives moderate changes on the calculated β_{tot} upon reduction. However, β_{tot} diminish upon reduction, contrary to what occurred for the oxidative counterpart. For $\mathbf{FeL}^{red}$ and $\mathbf{RuL}^{red}$, the role played by the organometallic moiety on the first hyperpolarizability is less significant than the observed for oxidized species. In fact, for $\mathbf{FeL}^{ox}$ and $\mathbf{RuL}^{ox}$, the main optical transition was clearly assigned to MLCT with a favorable geometry for metal−ligand interaction, whereas for $\mathbf{FeL}^{red}$ and $\mathbf{RuL}^{red}$ a contribution of a LMCT is observed besides an ILCT. In addition, the M−N≡C1 angle largely deviates from linearity, which does not lead to a favorable metal−ligand π-interaction in ground state. Indeed, the character and energies of these transitions are close to those found for $\mathbf{L}^{red}$. As a result, the values of first hyperpolarizabilities are expected to be similar. This is true for $\mathbf{FeL}^{red}$, but $\mathbf{RuL}^{red}$ has lower β_{tot}. For this complex, there is no clear dominant component contributing to β_{tot} (Supporting Information). Thus, the analysis of the first hyperpolarizability according to TLM formalism is not applicable, and it is difficult and discouraged to make reasonable comparisons with $\mathbf{FeL}^{red}$ and $\mathbf{L}^{red}$.

When considering the results obtained with B3LYP and M06 functionals, and contrary to the behavior found for CAM-B3LYP, β_{tot} clearly increases upon reduction, in particular for organometallic complexes. For example, B3LYP and M06 predict 1.52 and 1.79 eV, respectively, for $\mathbf{FeL}^{red}$. For the same complex, an energy of 2.04 eV results from the CAM-B3LYP functional. The main reason seems to be the underestimation of the main optical transition energies when B3LYP and M06 functional were used, as was discussed for the oxidized molecules. In addition, the character of the optical transition seems also to play a role. As an example, the significant molecular orbitals for $\mathbf{FeL}^{red}$, obtained using B3LYP, are depicted in Figure 9. The character of β orbitals is similar for

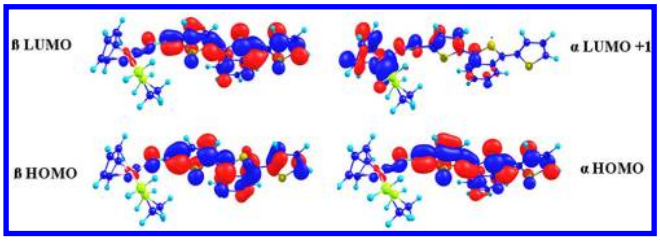

Figure 9. Molecular orbitals of $\mathbf{FeL}^{red}$ involved in the dominant optical transitions using B3LYP.

both CAM-B3LYP and B3LYP functionals. The main difference is on the optical transition involving α orbitals. Using B3LYP, the αL+1 orbital has a higher contribution of the organometallic moiety when compared to the αL+2 obtained with CAM-B3LYP. Thus, an enhanced contribution of LMCT is observed with B3LYP, which could lead to higher hyperpolarizabilities. The predicted energies of the main electronic transition using B3LYP and M06 for reduced species, in the range of 1.52−1.79 eV, are significantly higher than those obtained in oxidized molecules (0.83−1.03 eV) and, consequently, closer to the values found when using CAM-B3LYP functional. As mentioned above, for reduced species, the main electronic transitions can be assigned to ILCT and LMCT. Therefore, when compared to the oxidized species, lower charge separation results from the excitations. Thus, it is expected that B3LYP and M06 functionals could give less unrealistic results.

The overall results show that organometallic moieties play an important role in the NLO response with respect to the redox stimulus. The calculated data using B3LYP and M06 functionals shows, in general, similar results and/or trends, in particular on structural and optical data. As discussed above,

these functionals predicts (in an unrealistic manner) significant enhancement of second-order hyperpolarizabilities of the studied organometallic complexes through one-electron oxidation/reduction processes. The CAM-B3LYP functional, however, points to a more moderate effect and opposite effects on NLO response upon oxidation and reduction. For most of metal-containing compounds that have been studied for redox NLO switching, the changing on hyperpolarizability properties is, in fact, moderate: the largest experimental second-order NLO response ("on" form) is approximately 2 to 20-fold greater than the "off" form.[8] At this point, we have to reinforce the fact that in most of these systems there is a lowering of the hyperpolarizabilities upon a oxidation stimulus that is not the case in the present studied molecules, as has been clearly highlighted and explained above. Also, as indicated, this functional seems to predict more reliable structural, optical, and hyperpolarizability experimental data. Thus, it is reasonable to assume that NLO response trends upon redox stimulus obtained with CAM-B3LYP functional could be more realistic. Therefore, the studied complexes can be viewed as acting as redox NLO switchable, both using oxidative or reductive stimulus. However, the NLO switching is more effective using oxidation stimulus because larger differences on β_{tot} are observed between nonoxidized and oxidized species. Thus, **FeL**^{ox} and **RuL**^{ox} complexes can be viewed as the "on" form, whereas **FeL** and **RuL** can be viewed as the "off" form. In order to confirm this assumption, experimental studies for evaluation of NLO redox switching properties of these compounds are currently in progress.

4. CONCLUSIONS

The benzo[*c*]thiophene nitrile organometallic complexes of iron and ruthenium were found to be good candidate materials for second-order NLO switching by redox means. Both oxidative and reductive stimulus for NLO switching have been studied. In particular, oxidation of organometallic complexes can significantly enhance the second-order hyperpolarizabilities. The β_{tot} values indicate a clear dependence on the functional used for the calculations. CAM-B3LYP seems to predict more reliable structural, optical, and hyperpolarizabilitiy experimental data. B3LYP and M06 functionals predict significant enhancement of second-order hyperpolarizabilities of the studied organometallic complexes through redox stimulus, but β_{tot} seem to be clearly overestimated due to the shortcoming of these functionals in correct estimation of the energies of excitations with a long-range spatial extent. Thus, NLO response trends upon redox stimulus obtained with CAM-B3LYP might be more realistic. The use of this functional originates β_{tot} values of **RuL**^{ox} and **FeL**^{ox} 8.3 times and 5.5 times larger and of **RuL**^{red} and **FeL**^{red} 2.3 times and 1.2 times smaller than those of nonoxidized/reduced counterparts. TD-DFT calculations show that the enhancing/decreasing effect on the second-order NLO response upon oxidation/reduction is due to a change in the charge transfer pattern. In fact, in the oxidized form, the organometallic fragments play an important role on the hyperpolarizabilities because an effective low-energy MLCT electronic transition arises in the calculated optical spectra instead of a higher energy excitation, mainly with ILCT character, observed in nonoxidized/reduced and reduced counterparts. The switching values obtained by oxidation means indicate that these complexes may be used as "off−on" second-order NLO molecular switches materials, where **FeL**^{ox} and **RuL**^{ox} complexes can be viewed as the "on" form, whereas **FeL** and **RuL** can be viewed as the "off" form.

■ ASSOCIATED CONTENT

Supporting Information

Tables with detailed description of bond lengths and bond angles and ß tensors for all studies complexes. This material is available free of charge via the Internet at http://pubs.acs.org.

■ AUTHOR INFORMATION

Corresponding Author

*E-mail: pjgm@uevora.pt. Phone: +351 266745318. Fax: +351 26645303.

Notes

The authors declare no competing financial interest.

■ ACKNOWLEDGMENTS

The authors thank the FCT for funding of Project FCOMP-01-0124-FEDER-007433. Tiago Silva is also grateful for his Ph.D. grant.

■ REFERENCES

(1) Feringa, B. L. *Molecular Switches*; Ben L. Feringa, Ed.; Wiley-VCH; Weinheim, Germany; 2001.
(2) Irie, I. Photochromism: Memories and Switches − Introduction. *Chem. Rev.* **2000**, *100*, 1683−1890.
(3) Prasanna de Silva, A.; Nimal Gunaratne, H. Q.; Gunnlaugsson, T.; Huxley, A. J. M.; McCoy, C. P.; Rademacher, J. T.; Rice, T. E. Signaling recognition events with fluorescent sensors and switches. *Chem. Rev.* **1997**, *97*, 1515−1566.
(4) Sato, O. Optically switchable molecular solids: Photoinduced spin-crossover, photochromism and photoinduced magnetization. *Acc. Chem. Res.* **2003**, *36*, 692−700.
(5) Coe, B. Molecular materials possessing switchable quadratic nonlinear optical properties. *Chem.—Eur. J.* **1999**, *5*, 2464−2471.
(6) Asselberghs, I.; Clays, K.; Persoons, A.; Ward, M. D.; McCleverty, J. Switching of molecular second-order polarizability in solution. *J. Mater. Chem.* **2004**, *14*, 2831−2839.
(7) Coe, B. Switchable nonlinear optical metallochromophores with pyridinium electron acceptor groups. *Acc. Chem. Res.* **2006**, *39*, 383−393.
(8) Green, K. A.; Cifuentes, M. P.; Samoc, M.; Humphrey, M. G. Metal alkynyl complexes as switchable NLO systems. *Coord. Chem. Rev.* **2011**, *255*, 2530−2541.
(9) T. Weyland, T; Ledoux, I.; Brasselet, S.; Zyss, J.; Lapinte, C. Nonlinear optical properties of redox-active mono-, bi-, and trimetallic σ-acetylide complexes connected through a phenyl ring in the Cp*(dppe)Fe series. An example of electro-switchable NLO response. *Organometallics* **2000**, *19*, 5235−5237.
(10) Wahab, A.; Bhattacharya, M.; Ghosh, S.; Samuelson, A. G.; Das, Puspendu, K. Quadratic nonlinearity of one- and two-electron oxidized metalloporphyrins and their switching in solution. *J. Phys. Chem. B* **2008**, *112*, 2842−2847.
(11) Li, X.-J.; Sun, S.-L.; Ma, N.-N.; Sun, X.-X.; Yang, G.-C.; Qiu, Y.-Q. Theoretical investigations on electronic spectra and the redox-switchable second-order nonlinear optical responses of rhodium (I)-9-10-phenanthrenediimine complexes. *J. Mol. Graph. Mod.* **2012**, *33*, 19−25.
(12) Rao, V. P.; Jen, Alex K.-Y.; Wong, K. Y.; Drost, Kevin. J. Novel push-pull thiophenes for second-order nonlinear optical applications. *Tetrahedron Lett.* **1993**, *34*, 1747−1750.
(13) Hutchings, M. G.; Ferguson, I.; McGreen, D. J.; Morley, J. O.; Zyss, J.; Ledoux, I. Quadratic nonlinear optical properties of some donor-acceptor substituted thiophenes. *J. Chem. Soc., Perkin Trans. 2* **1995**, 171−176.

(14) Branger, C.; Lequan, M.; Lequan, R. M.; Barzoukas, M.; Fort, A. Boron derivatives containing bithiophene bridge as new materials for nonlinear optics. *J. Mater. Chem.* **1996**, *6*, 555−558.
(15) Chou, S.-S. P.; Sun, D.-J.; Lin, H.-C.; Yang, P.-K. Second-order nonlinearities and crystal structures of methylsulfonyl- and phenylsulfonyl-substituted thiophene imino dyes. *J. Chem. Soc., Chem. Commun.* **1996**, *9*, 1045−1046.
(16) Garcia., M. H.; Royer, S.; Robalo, M. P.; Romão Dias, A.; Tranchier, J.-P.; Chavignon, R.; Prim, D.; Auffrant, A.; Rose-Munch, F.; Rose, E.; Vaissermann, J.; Persoons, A.; Asselberghs, I. Synthesis, characterization of (arene)tricarbonylchromium complexes linked to cationic Fe and Ru derivatives and studies of first hyperpolarizabilities by hyper-rayleigh scattering. *Eur. J. Inorg. Chem.* **2003**, *21*, 3895−3904.
(17) Garcia, M. H.; Mendes, P. J.; Robalo, M. P.; Romão Dias, A.; Campo, J.; Wenseleers, W.; Goovaerts, E. Compromise between conjugation length and charge-transfer in nonlinear optical η^5-monocyclopentadienyliron(II) complexes with substituted oligothiophene nitrile ligands: Synthesis, electrochemical studies and first hyperpolarizabilities. *J. Organomet. Chem.* **2007**, *692*, 3027−3041.
(18) Garcia, M. H.; Florindo, P.; Piedade, M. F.; Duarte, M. T.; Robalo, M. P.; Heck, J.; Wittenburg, C.; Holtmann, J.; Licandro, E. Synthesis of organometallic Ru(II) and Fe(II) complexes containing fused rings hemi-helical ligands as chromophores. Evaluation of nonlinear optical properties by HRS. *J. Organomet. Chem.* **2008**, *693*, 2987−2999.
(19) Garcia, M. H.; Florindo, P.; Piedade, M. F.; Duarte, M. T.; Robalo, M. P.; Gooverts, E.; Wenseleers, W. Synthesis and sturctural characterization of ruthenium(II) and iron(II) complexes containing 1,2-di-(2-thienyl)-ethene derived ligands as chromophores. *J. Organomet. Chem.* **2009**, *694*, 433−445.
(20) Mendes, P. J.; Palace Carvalho, A. J.; Prates Ramalho, J. P. Role played by the organometallic fragment on the first hyperpolarizability of iron-acetylide complexes: A TD-DFT study. *J. Mol. Struct.: THEOCHEM* **2009**, *900*, 110−117.
(21) Xu, L.; Shao, X.; Cai, W. *J. Mol. Struct.: THEOCHEM* **2010**, *946*, 33−42.
(22) Hutchison, G. R.; Ratner, M. A.; Marks, T. J. Electronic structure and band gap in cationic heterocyclic oligomers. multidimensional analysis of the interplay of heteroatoms, substituents, molecular length, and charge on redox and transparency characteristics. *J. Phys. Chem. B* **2005**, *109*, 3126−3138.
(23) Qin, Y.; Kim, J. Y.; Frisble, C. D.; Hillmyer, M. A. Distannylated isothianaphthene: A versatile building block for low bandgap conjugated polymers. *Macromolecules* **2008**, *41*, 5563−5570.
(24) Frisch, M. J.; Trucks, G. W.; Schlegel, H. B.; Scuseria, G. E.; Robb, M. A; Cheeseman, J. R.; Scalmani, G.; Barone, V.; Mennucci, B.; Petersson, G. A.; Nakatsuji, H.; Caricato, M.; Li, X.; Hratchian, H. P.; Izmaylov, A. F.; Bloino, J.; Zheng, G.; Sonnenberg, J. L.; Hada, M.; Ehara, M.; Toyota, K.; Fukuda, R.; Hasegawa, J.; Ishida, M.; Nakajima, T.; Honda, Y.; Kitao, O.; Nakai, H.; Vreven, T.; Montgomery, J. A.; Peralta, J. E.; Ogliaro, F.; Bearpark, M.; Heyd, J. J.; Brothers, E.; Kudin, K. N.; Staroverov, V. N.; Kobayashi, R.; Normand, J.; Raghavachari, K.; Rendell, A.; Burant, J. C.; Iyengar, S. S.; Tomasi, J.; Cossi, M.; Rega, N.; Millam, J. M.; Klene, M.; Knox, J. E.; Cross, J. B.; Bakken, V.; Adamo, C.; Jaramillo, J.; Gomperts, R.; Stratmann, R. E.; Yazyev, O.; Austin, A. J.; Cammi, R.; Pomelli, C.; Ochterski, J. W.; Martin, R. L.; Morokuma, K.; Zakrzewski, V. G.; Voth, G. A.; Salvador, P.; Dannenberg, J. J.; Dapprich, S.; Daniels, A. D.; Farkas, O.; Foresman, J. B.; Ortiz, J. V.; Cioslowski, J.; Fox, D. J., Gaussian, Inc., Wallingford CT, 2009.
(25) Hay, P. J.; Wadt, W. R. Ab initio effective core potentials for molecular calculations. Potentials for the transition metal atoms Sc to Hg. *J. Chem. Phys.* **1985**, *82*, 270−283.
(26) Wadt, W. R.; Hay, P. J. Ab initio effective core potentials for molecular calculations. Potentials for main group elements Na to Bi. *J. Chem. Phys.* **1985**, *82*, 284−298.
(27) Hay, P. J.; Wadt, W. R. Ab initio effective core potentials for molecular calculations. Potential for K to Au including the outermost core orbitals. *J. Chem. Phys.* **1985**, *82*, 299−310.
(28) Dunning, T. H.; Hay, P. J. In *Modern Theoretical Chemistry*; Shaefer, H. F.; Plenum, Ed.; New York, 1976; Vol. *3*, pp 1−28.
(29) Check, C. E.; Faust, T. O.; Bailey, J. M.; Wright, B. J.; Gilbert, T. M.; Sunderlin, L. S. Addiction of polarization and diffuse functions to the LANL2DZ basis set for P-block elements. *J. Phys. Chem. A* **2001**, *105*, 8111−8116.
(30) Feller, D. The role of databases in support of computational chemistry calculations. *J. Comput. Chem.* **1996**, *17*, 1571−1586.
(31) Schuchardt, K. L.; Didier, B. T.; Elsethagen, T.; Sun, L.; Gurumoorthi, V.; Chase, J.; Li, J.; Windus, T. L. Basis set exchange: A community database for computational sciences. *J. Chem. Inf. Model.* **2007**, *47*, 1045−1052.
(32) Kanis, D. R.; Ratner, M. A.; Marks, T. J. Design and construction of molecular assemblies with large second-order optical nonlinearities. quantum aspects. *Chem. Rev.* **1994**, *94*, 195−242.
(33) Gross, E. K. U.; Dobson, J. F.; Petersilka, M. *Density Functional Theory*; Nalawejski, R. F., Ed.; Springer: Berlin, Germany, 1996; Vol. *181*.
(34) Casida, M. E.; Jamorski, C.; Casida, K. C.; Salahub, D. R. Molecular excitation energies to high-lying bound states form time-dependent density functional response theory: Characterization and correction of the time-dependent local density approximation ionization threshold. *J. Chem. Phys.* **1998**, *108*, 4439−4450.
(35) Dreuw, A.; Head-Gordon, M. Single-reference ab initio methods for the calculation of excited states of large molecules. *Chem. Rev.* **2005**, *105*, 4009−4037.
(36) O'Boyle, N. M.; Tenderholt, A. L.; Langner, K. M. cclib: A library for package-independent computational chemistry algorithms. *J. Comput. Chem.* **2008**, *29*, 839−845.
(37) Zhurko G. A.; Zhurko D. A. *ChemCraft: Tool for Treatment of Chemical Data*, build 342. http://www.chemcraftprog.com, 2010.
(38) Becke, A. D. Density-functional thermochemistry. III. The role of exact exchange. *J. Chem. Phys.* **1993**, *98*, 5648−5653.
(39) Lee, C.; Yang, W.; Parr, R. G. Development of the Colle−Salvetti correlation-energy formula into a functional of the electronic density. *Phys. Rev. B* **1988**, *37*, 785−789.
(40) Yanai, T.; Tew, D. P.; Handy, N. C.; New, A Hybrid exchange-correlation functional using the Coulomb-attenuating method (CAM-B3LYP). *Chem. Phys. Lett.* **2004**, *393*, 51−57.
(41) Zhao, Y.; Truhlar, G. D. The M06 suite of density functionals for main group thermochemistry, themochemical kinetics, noncovalent interactions, excited states and trasition elements: Two new functionals and systematic testing of four M06-class functionals and 12 other functionals. *Theor. Chem. Acc.* **2004**, *120*, 215−241.
(42) Zhao, Y.; Truhlar, G. D. Attractive noncovalent interactions in the mechanism of Grubbs second-generation Ru catalysts for olefin metethesis. *Org. Lett.* **2007**, *9*, 1967−1970.
(43) Schultz, N.; Zhao, Y.; Truhlar, G. D. Density functionals for inorganometallic and organometallic chemistry. *J. Phys. Chem. A* **2005**, *109*, 11127−11143.
(44) Harvey, J. N. On the accuracy of density functional theory in transition metal chemistry. *Annu. Rep. Prog. Chem. Sect. C: Phys. Chem.* **2006**, *102*, 203−226.
(45) Zhao, Y; Truhlar, D. G. Density functionals with broad applicability in chemistry. *Acc. Chem. Res.* **2008**, *41*, 157−167.
(46) Liu, C.-G.; Guan, X.-H.; Su, Z.-M. Computational study on redox-switchable 2D second-order nonlinear optical properties of push-pull mono-tetrathiafulvalene-bis(salicylaldiminato) Zn(II) Schiff base complexes. *J. Phys. Chem. C* **2011**, *115*, 6024−6032.
(47) Muhammad, S.; Xu, H.; Saeed, M. S.; Janjua, A.; Su, Z.; Nadeem, M. Quantum chemical study of benzimidazole derivatives to tune the second-order nonlinear optical molecular switching by proton abstraction. *Phys. Chem. Chem. Phys.* **2010**, *12*, 4791−4799.
(48) Zhao, H.-B.; Qiu, Y.-Q.; Liu, C.-G.; Sun, S.-L.; Liu, Y.; Wang, R.-S. Redox-swichtable second-order nonlinear optical responses of TEMPO-dithiolate ligand and (TEMPOdt)M complexes (M=Pt, Pd). *J. Organomet. Chem.* **2010**, *695*, 2251−2257.
(49) Franzen, P. L.; Zilio, S. C.; Machado, A. E. H.; Madurro, J. M.; Brito-Madurro, A. G.; Ueno, L. T.; Sampaio, R. N.; Barbosa Neto, N.

M. Experimental and theoretical investigation of first hyperpolarizability in aminophenols. *J. Mol. Struct.* **2008**, *892*, 254−260.
(50) Mang, C.; Wu, K. First hyperpolarizabilities of vinylogue organometallic sesquifulvalene. *Int. J. Quantum Chem.* **2006**, *106*, 2529−2535.
(51) Cardoso, C.; Abreu, P. E.; Nogueira, F. Strucutre dependence of hyperpolarizability on octopolar molecules. *J. Chem. Theory Comput.* **2009**, *5*, 850−858.
(52) R. J. Magyar, R. J.; Tretiak, S. Dependence of spurius charge-transfer excited states on orbital exchange in TDDFT: Large molecules and clusters. *J. Chem. Theory Comput.* **2007**, *3*, 976−987.
(53) Ferrighi, L.; Frediani, L.; Cappelli, C.; Sałek, P.; Ågren, H.; Helgaker, T.; Ruud, K. Density-functional-theory study of the electric-field-induced second harmonic generation (EFISHG) pf push-pull phenylpolyenes in solution. *Chem. Phys. Lett.* **2006**, *425*, 267−272.
(54) Peach, M. J. G.; Helgaker, T.; Sałek, P.; Keal, T. W.; Lutnaes, O. B.; Tozer, D. J.; Handy, N. C. Assessment of a Coulomb-attenuated exchange-correlation energy functional. *Phys. Chem. Chem. Phys.* **2006**, *8*, 558−562.
(55) Jacquemin, D.; Perpete, E. A.; Scalmani, G.; Frisch, M. J.; Kobayashi, R.; Adamo, C. Assessment of the efficiency of long-range corrected functionals for some properties of large compounds. *J. Chem. Phys.* **2007**, *126*, 144105−144117.
(56) Jacquemin, D.; Perpete, E; Medved, M.; Scalmani, G.; Frisch, M. J.; Kobayashi, R.; Adamo, C. First hyperpolarizability of polymethineimine with long-range corrected functionals. *J. Chem. Phys.* **2007**, *126*, 191108−191112.
(57) Jacquemin, D.; Perpète, E. A.; Scuseria, G. E.; Ciofini, I.; Adamo, C. TD-DFT performance for the visible absortion spectra of organic dyes: Conventional versus long-range hybrids. *J. Chem. Theory Comput.* **2008**, *4*, 123−135.
(58) Limacher, P. A.; Mikkelsen, K. W.; Luthi, H. P. On the Accurate calculation of polarizabilities and second hyperpolarizabilities of polyacetylene oligomer chains using the CAM-B3LYP density functional. *J. Chem. Phys.* **2009**, *130*, 194114−194121.
(59) Corozzi, A.; Mennucci, B.; Cammi, R.; Tomasi, J. Structure versus solvent effects on nonlinear optical properties of push-pull systems: A quantum-mechanical study based on a polarizable continuum model. *J. Phys. Chem. A* **2009**, *113*, 14774−14784.
(60) Valero, R.; Costa, R.; Moreira, I. P. R.; Truhlar, D. G.; Illas, F. Performance of tthe M06 family of exchange-correlation functionals for predicting magnetic coupling in organic and inorganic molecules. *J. Chem. Phys.* **2008**, *128*, 114103−114111.
(61) Jacquemin, D.; Perpète, E. A.; Ciofini, I.; Adamo, C.; Valero, R.; Zhao, Y.; Truhlar, D. G. On the performance of the M06 family of density functionals for electronic excitation energies. *J. Chem. Theory Comput.* **2010**, *6*, 2071−2085.
(62) Cordiner, R. L.; Corcoran, D.; Yufit, D. S.; Goeta, A. E.; Howard, J. A. K.; Low, P. J. Cyanoacetylene and cyanoacetylides: Versatile ligands in organometallic chemistry. *Dalton Trans.* **2003**, *18*, 3541−3549.
(63) Garcia, M. H.; Rodrigues, J. C.; Romão Dias, A.; Piedade, M. F.; Duarte, M. T.; Robalo, M. P.; Lopes, N. Second harmonic generation of η^5-monocyclopentadienyl ruthenium p-benzonitrile derivatives by Kurtz powder technique. Crystal and molecular structure determinations of $[Ru(\eta^5\text{-}C_5H_5)((+)\text{-}DIOP)(p\text{-}NCC_6H_4NO2)][X]$, X = PF_6^-, $CF_3SO_3^-$ and $[Ru(\eta^5\text{-}C_5H_5)((+)\text{-}DIOP)(NCCH_3)][PF_6]$. *J. Organomet. Chem.* **2001**, *632*, 133−144.
(64) Garcia, M. H.; Teixeira, A. P. S.; Romão Dias, A.; Piedade, M. F.; Duarte, M. T. Synthesis of new donor/acceptor η^5-cyclopentadienyl and η^5-indenyliron(II) complexes with p-benzonitrile derivatives. Crystal structures of $[Fe(\eta^5\text{-}C_5H_5)(CO)(P(OC_6H_5)_3)(p\text{-}NCC_6H_4NO_2)][BF_4]\cdot CH_2Cl_2$ and $[Fe(\eta^5\text{-}C_9H_7)(CO)(P(OC_6H_5)_3)(p\text{-}NCC_6H_4NO_2)][BF_4]$. *J. Organomet. Chem.* **2001**, *632*, 145−156.
(65) Peach, M. J. G.; Tellgren, E. I.; Salek, P.; Helgaker, T; Tozer, D. J. Structural and electronic properties of polyacetylene and polyyne from hybrid and coulomb-attenuated density functionals. *J. Phys. Chem. A* **2007**, *111*, 11930−11935.
(66) Jacqumin, D.; Adamo, C. Bond length alternation of conjugated oligomers: Wave function and DFT benchmarks. *J. Chem. Theory Comp.* **2011**, *7*, 369−376.
(67) Oudar, J. L.; Chemla, D. S. Hyperpolarizabilities of the nitroanilines and their relations to the excited state dipole moment. *J. Chem. Phys.* **1977**, *66*, 2664−2269.
(68) Silva, T. J. L.; Mendes, Paulo J. G.; Garcia, M. H., Ramalho, J. P. Prates; Carvalho, A. J. Palace, Organometallic Complexes for Nonlinear Optical Switching: DFT Evaluation of the B3LYP, CAM-B3LYP and M06 Functionals. In Abstracts of Papers of the Ninth Triennial Congress of the World Association of Theoretical and Computational Chemists WATOC 2011, Santiago de Compostela, Spain, July 17−22, 2011; Abstract PII 061.
(69) Roncali, J. Molecular engineering of the band-gap of π-conjugated systems: Facing technological applications. *Macromol. Rapid Commun.* **2007**, *28*, 1761−1775.
(70) Denis, R.; Toupet, L.; Paul, F.; Lapinte, C. Electron-rich piano-stool iron σ-acetylides bearing a functional aryl group. Synthesis and characterization of iron(II) and iron(III) complexes. *Organometallics* **2000**, *19*, 4240−4251.
(71) Bruce, M. I.; Ellis, B. G.; Low, P. J.; Skelton, B. W.; White, A. H. Synthesis, structures, and spectro-electrochemistry of {Cp*(PP)Ru}-C≡CC≡C{Ru(PP)Cp*} (PP= dppm, dppe) and their mono- and dications. *Organometallics* **2003**, *22*, 3184−3198.
(72) Paul, F.; Toupet, L.; Thépot, J.-Y.; Costuas, K.; Halet, J.-F.; Lapinte, C. Electron-rich piano-stool iron σ-acetylides. Electronic structures of alkynyl iron(III) radical cations. *Organometallics* **2005**, *24*, 5464−5479.
(73) Ruzsinszky, A.; Perdew, J. P.; Csonka, G. I.; Scuseria, G. E.; Vydrov, O. A. Understanding and correcting the self-interaction error in the electrical response oh hydrogen chains. *Phys. Rev. A* **2008**, *77*, 60502−60506.
(74) Vydrov, O. A.; Scuseria, G. E.; Perdew, J. P.; Ruzsinszky, A.; Csonka, G. I. Scaling down the Pardew-Zunger self-interaction correction in many-electron regions. *J. Chem. Phys.* **2006**, *124*, 94108−94116.
(75) Ruzsinszky, A.; Perdew, J. P.; Csonka, G. I.; Vydrov, O. A.; Scuseria, G. E. Density functionals that are one- and two- are not always many-electron self-interaction-free, as shown for H_2^+, He_2^+, LiH^+ and Ne_2. *J. Chem. Phys.* **2007**, *126*, 104102−104110.
(76) Champagne, B.; Perpete, E. A.; Jacquemin, D.; van Gisbergen, S. J. A.; Baerends, E. J.; Soubra-Ghaoui, C.; Robins, K. A.; Kirtman, B. Assessment of conventional density functional schemes for computing the dipole moment and (hyper)polarizabilities of push-pull π-conjugated systems. *J. Phys. Chem. A* **2000**, *104*, 4755−4763.
(77) Dreuw, A.; Head-Gordon, M. Failure of time-dependent density functional theory for long-range charge-transfer excited-states: The zincbacteriochlorin-bacteriochlorin and bacteriochlorophyll-spheriodene complexes. *J. Am. Chem. Soc.* **2004**, *126*, 4007−4016.
(78) Powell, C. E.; Humphrey, M. G. Nonlinear optical properties of transition metal acetylides and their derivatives. *Coord. Chem. Rev.* **2004**, *248*, 725−756.
(79) Green, K. A.; Cifuentes, M. P.; Samoc, M.; Humphrey, M. G. Synthesis and NLO properties of metal alkynyl dendrimers. *Coord. Chem. Rev.* **2011**, *255*, 2025−2038.
(80) Babgi, B.; Rigamonti, L.; Cifuentes, M. P.; Corkery, T.; Christopher; Randles, Michael, D.; Schwich, T.; Petrie, S.; Stranger, R.; Teshome, A.; Asselberghs, I.; Clays, K.; Samoc, M.; Humphrey, M. G. Length-dependent convergence and saturation behavior of electrochemichal, linear optical, quadratic nonlinear optical, and cubic nonlinear optical properties of dipolar alkynylruthenium complexes with oligo(phenyleneethynylene) bridges. *J. Am. Chem. Soc.* **2009**, *131*, 10293−10307.
(81) Garcia, M. H.; Robalo, M. P.; Dias, A. R.; Duarte, M. T.; Wenseleers, W.; Aerts, G.; Goovaerts, E.; Cifuentes, M. P.; Hurst, S.; Humphrey, M. G.; Samoc, M.; Luther-Davis, B. Synthesis and nonlinear optical properties of η^5-monocyclopentadienyliron(II) acetylides derivatives. X-ray crystal structures of $[Fe(\eta^5\text{-}C_5H_5)(DPPE)(p\text{-}C{\equiv}CC_6H_4NO_2)]$ and [Fe-

(η^5-C_5H_5)(DPPE)((E)(*p*-C≡CC_6H_4C(H)=C(H)$C_6H_4NO_2$)]. *Organometallics* **2002**, *21*, 2107−2118.

(82) Wenseleers, W.; Gerbrandji, A. W.; Goovaerts, E.; Garcia, M. H.; Robalo, M. P.; Mendes, P. J.; Rodrigues, J. C; Romão Dias, A. Hyper-rayleigh scattering study of η^5-monocyclopentadienyl-metal complexes for second-order optical materials. *J. Mater. Chem.* **1998**, *8*, 925−930.

(83) Liu, Y.; Liu, C.-G.; Sun, S.-L.; Yang, G.-C.; Qiu, Y.-Q. Redox-switching second-order nonlinear optical responses of N^N^N ruthenium complexes. *Comput. Theor. Chem.* **2012**, *979*, 112−118.